144–157 *Nucleic Acids Research, 2009, Vol. 37, No. 1* *Published online 25 November 2008*
doi:10.1093/nar/gkn900

The class E floral homeotic protein SEPALLATA3 is sufficient to loop DNA in 'floral quartet'-like complexes *in vitro*

Rainer Melzer[1], Wim Verelst[2] and Günter Theißen[1,*]

[1]Department of Genetics, Friedrich Schiller University Jena, Philosophenweg 12, D-07743 Jena and [2]Department of Molecular Plant Genetics, Max Planck Institute for Plant Breeding Research, Carl von Linné Weg 10, D-50829 Köln, Germany

Received October 1, 2008; Revised October 23, 2008; Accepted October 24, 2008

ABSTRACT

The organs of a eudicot flower are specified by four functional classes, termed class A, B, C and E, of MADS domain transcription factors. The combinatorial formation of tetrameric complexes, so called 'floral quartets', between these classes is widely believed to represent the molecular basis of floral organ identity specification. As constituents of all complexes, the class E floral homeotic proteins are thought to be of critical relevance for the formation of floral quartets. However, experimental support for tetrameric complex formation remains scarce. Here we provide physico-chemical evidence that *in vitro* homotetramers of the class E floral homeotic protein SEPALLATA3 from *Arabidopsis thaliana* bind cooperatively to two sequence elements termed 'CArG boxes' in a phase-dependent manner involving DNA looping. We further show that the N-terminal part of SEPALLATA3 lacking K3, a subdomain of the protein–protein interactions mediating K domain, and the C-terminal domain, is sufficient for protein dimerization, but not for tetramer formation and cooperative DNA binding. We hypothesize that the capacity of class E MADS domain proteins to form tetrameric complexes contributes significantly to the formation of floral quartets. Our findings further suggest that the spacing and phasing of CArG boxes are important parameters in the molecular mechanism by which floral homeotic proteins achieve target gene specificity.

INTRODUCTION

Homeotic selector genes are key regulators during development that determine the identity of whole organs or segments. Prominent examples are the Hox genes that manifest positional information along the anterior–posterior axis of animals (1,2). In plants, homeotic selector genes specifying floral organ identities—so called floral homeotic genes—are especially well studied. Initially, three classes A, B and C of floral homeotic genes have been identified by mutant analysis (3,4). How the combinatorial interaction among these different classes of floral homeotic genes governs organ identity is explained by the ABC model, according to which class A genes alone determine sepal identity, class A and class B genes together specify petal identity, class B and class C genes together govern stamen (male reproductive organ) development and a class C gene alone determines carpel (female reproductive organ) development (3,4). In *Arabidopsis thaliana*, the class A genes are *APETALA1* (*AP1*) and *APETALA2* (*AP2*), the class B genes are *APETALA3* (*AP3*) and *PISTILLATA* (*PI*) and the only class C gene is *AGAMOUS* (*AG*) (5–9). With the exception of *AP2*, all of these genes encode MADS domain transcription factors.

Although class A, B and C floral homeotic genes are necessary for floral organ development, ectopic expression experiments showed that they are not sufficient to fully induce floral organ formation outside of the flower (10–12). This indicated that other factors involved in the determination of floral organ identity remained to be discovered (10). Indeed, reverse genetics analysis in *A. thaliana* revealed yet another group of largely redundant MADS box genes, termed *SEPALLATA1* (*SEP1*),

*To whom correspondence should be addressed. Tel: +49 3641 949550; Fax: +49 3641 949 552; Email: guenter.theissen@uni-jena.de
Present address:
Wim Verelst, VIB Department of Plant Systems Biology, Ghent University, Technologiepark 927, B-9052 Ghent, Belgium

SEP2, *SEP3* and *SEP4* (also known as *AGL2*, *AGL4*, *AGL9* and *AGL3*, respectively), as being important denominators for the identity of all floral organs (13,14). Because the term 'class D genes' was meanwhile assigned to genes important for ovule development, the *SEP* genes were defined as 'class E genes' (15). Simultaneous disruption of *SEP1*, *SEP2* and *SEP3* leads to the development of sepals rather than petals, stamens and carpels (hence the name 'SEPALLATA') (13), while the complete disruption of the class E gene function (in *sep1 sep2 sep3 sep4* quadruple mutants) leads to the transformation of all floral organs into vegetative leaves (14). Strikingly, ectopic expression of the class E gene *SEP3* together with class B genes, or with class B and class C genes, in *Arabidopsis* leads to the development of leaf primordia into petaloid or staminoid organs, respectively, implying that these combinations represent the set of master control genes sufficient to direct stamen and petal development (16). Similarly, ectopic expression of SEP2 together with AP3 and PI leads to a partial conversion of cauline leaves into petals, and constitutive expression of SEP3 and SEP2 together with AP1, AP3 and PI leads to a nearly complete conversion of rosette leaves into petals (17).

It was also shown that the class E floral homeotic protein SEP3 interacts with the class B proteins AP3 and PI in yeast three-hybrid assays (16). Furthermore, evidence was presented suggesting that the class B proteins DEFICIENS and GLOBOSA from *Antirrhinum majus* (snapdragon) bind in a complex together with the class A-related protein SQUAMOSA to DNA probes containing two appropriate *cis*-regulatory DNA elements, so called CArG boxes (for 'C-Arich-G', consensus sequence $5'$-CC(A/T)$_6$GG-$3'$) (18).

These findings all support the 'floral quartet model', suggesting that higher order complexes of MADS domain proteins specify the identity of the different floral organs (15,19). The floral quartet model predicts that the genetic interactions hypothesized by the ABC model are molecularly manifested by the formation of tetrameric protein complexes that include class E floral homeotic proteins. According to the quartet model, these tetrameric complexes are formed by binding of two MADS domain protein dimers to two nearby CArG boxes and looping of the intervening DNA (15,19). In this way, complexes of two AP1 and two SEP molecules specify sepals, complexes of AP1, SEP, AP3 and PI specify petals, complexes of SEP, AP3, PI and AG specify stamens and complexes comprising two SEP and two AG molecules specify carpels (15,19,20). Intriguingly, at least one SEP molecule is present in each of these complexes. Meanwhile, even more tetrameric MADS complexes have been described or predicted for other kinds of organs and tissues, such as ovules, the endothelium and the floral meristem (21–23), again always containing at least one SEP molecule.

Due to their predicted ubiquitous presence in floral homeotic protein complexes, SEP proteins are of special interest for further research. Among the four SEP proteins of *A. thaliana*, SEP3 is the one that is characterized best (14,16,17,21,23,24). Accumulating evidence suggests that the *SEP* genes are not completely redundant and that *SEP3* has a developmental role more prominent than that of the other *SEP* genes. For example, one copy of *SEP3* is sufficient to promote ovule development in a *sep1 sep2* background, whereas one copy of *SEP1* or *SEP2* fails to promote ovule identity in a *sep2 sep3* and *sep1 sep3* background, respectively (21). Also for floral organ development, SEP3 might be more critical than other SEP proteins. The *sep3* mutants, for example, resemble intermediate *ap1* mutants with a partial conversion of petals into sepals (24), whereas in *sep1 sep2 sep4* triple mutants floral organ development is like in the wild type (14).

In addition, yeast two-hybrid and yeast three-hybrid screens with AP1 or AP3-PI as bait proteins identified SEP3 but not other SEP proteins as interaction partners (16,24). Moreover, SEP3 has a transcriptional activation potential that exceeds that of SEP1 and SEP2 (16).

A more prominent role of SEP3 compared to the other SEP proteins is in line with phylogenetic studies suggesting that a duplication near the base of the angiosperms about 300 million years ago gave rise to two SEP lineages, one that contains *SEP3* and another one that underwent at least two more duplication events resulting in *SEP1, SEP2* and *SEP4* (25). Thus, *SEP3* evolved much longer than the other *SEP* genes and may thus during this time have acquired functions that distinguishes it from the other *SEP* genes.

Taken together, ample evidence suggests that SEP3 is the most important class E floral homeotic protein, with functions in floral meristem identity (23,24), floral organ identity (13,14,17) and ovule development (21,22). It thus appears timely to analyse the biochemical properties of SEP3 and how it interacts with DNA. This is especially evident as some essential assumptions of the floral quartet model—the stoichiometry of the protein complexes, the number of CArG boxes being involved and the looping of DNA to bring them into close vicinity—have not been confirmed experimentally yet, so that other mechanisms of floral homeotic protein function cannot be excluded (26,27).

Here, we use an *in vitro* approach to determine the protein–DNA interaction properties of SEP3. By using different suitably designed DNA fragments, we were able to reveal several unexpected intrinsic binding characteristics of SEP3. It turned out that homotetramers of SEP3 alone can bind cooperatively to two CArG boxes in a phase-dependent manner involving DNA looping, thus supporting some of the major tenets of the floral quartet model. Our findings suggest that quartet formation does not require the interaction of different floral homeotic proteins but is facilitated by an intrinsic capacity of SEP3 to tetramerize.

MATERIALS AND METHODS

Cloning of SEP3 and SEP3ΔK3C

The *SEP3* and *SEP3ΔK3C* cDNAs (GI:2345157) were amplified via PCR and cloned into pTNT (Promega; Mannheim, Germany) using EcoRI and SalI recognition sites. *SEP3ΔC* was cloned into pSPUTK using NcoI and

EcoRI recognition sites. The C-terminally truncated proteins SEP3ΔK3C and SEP3ΔC have a length of 152 and 188 amino acids, respectively, in contrast to the wild-type protein, which is 251 amino acids long.

DNA binding site probes

The CArG box sequence used in this study was derived from the regulatory intron of *AGAMOUS* (sequence 5′-GAAATTTAATTATATTCCAAATAAGGAAAGTATGGAACGTT-3′, the CArG box is underlined) (22). The respective double stranded oligonucleotide was cloned into both the SalI- and EcoRV recognition sites of pBluescript II SK(+). The 5′-overhangs produced by SalI digestion were treated with Klenow enzyme prior to blunt-end cloning. Digestion with XhoI and XbaI yielded a DNA fragment containing two CArG boxes spaced by 63 bp. Probes containing one CArG box only were constructed by cloning an oligonucleotide that had the same base composition as the oligonucleotide carrying the CArG box but in a randomized order into either the SalI or EcoRV site and the oligonucleotide encoding the CArG box into the remaining site. Digestion with XhoI and XbaI yielded a DNA fragment on which the CArG box was more peripherally (when cloned into the SalI recognition site) or more centrally (when cloned into the EcoRV recognition site) located.

Sequencing revealed that the orientation of the oligonucleotide with the randomized base composition cloned in the SalI site was reversed compared to the oligonucleotide cloned in the EcoRV site, but this was assumed to be of no relevance for the experiments performed and the conclusions drawn.

To construct probes in which the phasing between the two CArG boxes varied, linker sequences of different length were introduced into ClaI/HindIII sites between the two CArG boxes. Radioactive labelling was performed according to standard protocols (28).

Sequences of the oligonucleotides used can be found in Supplementary Table S1.

In vitro translation and electrophoretic mobility shift assays

In vitro translation was done using the SP6 TNT QuickCoupled Transcription/Translation mix (Promega). After *in vitro* translation, proteins were either used directly for electrophoretic mobility shift assay (EMSA) or shock-frozen in liquid nitrogen and stored at −70°C. In some experiments ^{35}S-methionine was used for radioactive labelling of proteins. The binding buffer used for gel retardation was similar to the one decribed by Egea-Cortines *et al.* (18). Briefly, for the protein–DNA binding reaction, 3 µl of a binding buffer containing 5.6 mM EDTA pH 8, 1.2 µg/µl BSA, 36 mM HEPES pH 7.2, 3.6 mM DTT, 690 ng salmon sperm DNA, 5.2 mM spermidine, 10% (w/v) CHAPS and 17.2% glycerol was incubated with various amounts of protein and a DNA probe in a total volume of 12–13 µl. For inferring cooperative binding, amounts of *in vitro* translated protein used were usually 0.05 µl, 0.1 µl, 0.2 µl, 0.4 µl, 0.6 µl, 0.8 µl, 1.2 µl, 1.5 µl, 2 µl, 3 µl, 4 µl, 6 µl and 10 µl. For other analyses (phasing, circular permutation and stoichiometry) generally between 0.4 µl and 4 µl of *in vitro* translated proteins, depending on the signal intensity desired, were used. Concentration of the DNA probe was generally ≤0.1 nM. When unlabelled DNA was used, concentration was between 10 nM and 40 nM. Variations in the amount of *in vitro* translated protein added were compensated by adding according volumes of BSA (10 µg/µl). Protein and DNA were co-incubated for at least 5 h on ice in the binding cocktail to allow the reaction to reach equilibrium. Ten microlitres of the binding reaction were loaded on a 0.5× TBE polyacrylamide gel that was pre-run for about 30 min. Gel run was performed at 7.5 V/cm for about 4 h. After gel drying, the signals were analysed by autoradiography or phosphorimaging.

Calculation of cooperativity constants

To estimate cooperative binding, we used equations essentially as described (29,30):

$$[Y_0] = \frac{1}{1 + (2/K_{d1})[P_2] + (1/(K_{d1}K_{d2}))[P_2]^2} \quad \mathbf{1}$$

$$[Y_2] = \frac{(2/K_{d1})[P_2]}{1 + (2/K_{d1})[P_2] + (1/(K_{d1}K_{d2}))[P_2]^2} \quad \mathbf{2}$$

$$[Y_4] = \frac{(1/(K_{d1}K_{d2}))[P_2]^2}{1 + (2/K_{d1})[P_2] + (1/(K_{d1}K_{d2}))[P_2]^2} \quad \mathbf{3}$$

$[Y_0]$, $[Y_2]$ and $[Y_4]$ describe relative concentrations of DNA configurations in which no, two or four proteins are bound to the DNA fragment. K_{d1} is the dissociation constant for binding of a protein dimer to one of the two CArG boxes (dissociation constants for protein binding to either of the two identical CArG boxes were assumed to be the same). K_{d2} denotes the dissociation constant for binding of a protein dimer to a DNA fragment on which one CArG box is already occupied (Figure 1B). As the proteins were produced by *in vitro* translation, the exact protein concentration is not known. We therefore used the amount M of *in vitro* translation mixture added to the binding reaction as a proxy for the concentration of protein dimers $[P_2]$ by assuming that

$$[P_2] = a[M], \quad \mathbf{4}$$

where a is a constant of proportionality. This implies that $[P_2]$ increases linearly with [M]. This approximation seems to be justified by the reasonable fit of our data to the graphs produced. (R^2 values usually were between 0.85 and 0.99, except for the $[Y_2]$ graphs of SEP3 and SEP3ΔC, where they varied between 0.51 and 0.77, probably due to difficulties to quantify the weak signals. If, what rarely happened, gel quantification was so difficult that one of the graphs yielded an R^2 value ≤0.5, these gels were excluded from the analysis.)

We also calculated K_{d1}/K_{d2} ratios by assuming that the concentration of protein monomers [P] rather than

that of dimers increases linearly with the amount of *in vitro* translation mixture added, i.e.

$$[P] = b[M], \quad 5$$

where b is a constant of proportionality. Dimerization prior to DNA binding was incorporated in Equations (1–3) by making the substitution

$$[P_2] = \frac{[P]^2}{K_{di}}, \quad 6$$

thus yielding

$$[Y_{0'}] = \frac{1}{1 + (2/K_{d1'})[P]^2 + (1/(K_{d1'}K_{d2'}))[P]^4} \quad 7$$

$$[Y_{2'}] = \frac{(2/K_{d1'})[P]^2}{1 + (2/K_{d1'})[P]^2 + (1/(K_{d1'}K_{d2'}))[P]^4} \quad 8$$

$$[Y_{4'}] = \frac{(1/(K_{d1}K_{d2}))[P]^4}{1 + (2/K_{d1'})[P]^2 + (1/(K_{d1'}K_{d2'}))[P]^4}, \quad 9$$

with

$$K_{d1'} = K_{d1}K_{di} \quad 10$$

$$K_{d2'} = K_{d2}K_{di} \quad 11$$

In most cases, the fit Equations (7–9) yielded were not as good as the ones obtained with Equations (1–3) as judged form the R^2 values of the individual graphs. For some cases of SEP3ΔK3C, the fit obtained with Equations (7–9) yielded higher R^2 values than that obtained with Equations (1–3) (data not shown). However, the resulting K_{d1}/K_{d2} ratios obtained for these data sets were always smaller when using Equations (7–9) compared to the ones obtained with Equations (1–3), and therefore rather increased the difference seen in cooperative binding between SEP3 and SEP3ΔC compared to SEP3ΔK3C. We therefore consider our approach to calculate K_{d1}/K_{d2} ratios by always using Equations (1–3) as a conservative estimate with respect to the differences between the different K_{d1}/K_{d2} values.

Data obtained from the gel shift experiments were fitted to the equations with the systemfit package implemented in R 2.6 (R development core team 2007).

Circular permutation analyses

Probe preparation was done as described (31). About 1000–5000 c.p.m. of labelled DNA was used per binding reaction. Sequence of the oligonucleotide encoding the CArG box that was cloned into the SalI/XbaI site of pBend2 (32) can be found in Supplementary Table S1. Bending angles were calculated as described (33–35).

Bimolecular fluorescence complementation analyses

Bimolecular fluorescence complementation (BiFC) analyses were performed as described (36,37). Pictures shown were taken 3–4 days after *Agrobacterium* infiltration using a fluorescence microscope equipped with appropriate filter cubes. Signals were also checked using a confocal laser scanning microscope.

DNase I footprinting

Protein–DNA incubation was performed as described for EMSA. About 10 000 c.p.m. of DNA labelled according to standard protocols (28) and 5–10 µl of *in vitro* translated protein were used per reaction. As for the EMSA analyses, the total reaction volume was 12–13 µl. After incubation, 2 µl DNase I (~5 U/µl in 9 mM HEPES, pH 7.2, 30 mM $MgCl_2$, 5 mM $CaCl_2$ and 0.1 mg/ml BSA) were added and incubated on ice for 30 s. The reaction was stopped by addition of 1 µl 500 mM EDTA. Free DNA was separated from protein–DNA complexes on a native 5% polyacrylamide gel. After gel run, bands were excised, the DNA eluted and resolved on a sequencing gel. After gel drying, the signals were analysed by phosphorimaging.

The A + G ladder was prepared by chemical sequencing essentially as described (38).

RESULTS

Four SEP3 proteins bind cooperatively to a DNA fragment carrying two CArG boxes

We used EMSAs to determine the stoichiometry of a SEP3–DNA complex. It is known that MADS domain proteins bind as dimers to DNA sequences termed CArG boxes [consensus sequence 5′-CC(A/T)$_6$GG-3′] (31,39–47). To test whether this also applies to SEP3, we incubated a mixture of a full-length and a C-terminal truncated (SEP3ΔC) *in vitro* translated SEP3 protein with a DNA fragment carrying one CArG box (Figure 1A). The sequence of the CArG box was derived from the regulatory intron of *AGAMOUS* (see Materials and methods section). If both SEP3 and SEP3ΔC bind as homodimers to DNA, an intermediate shift representing the SEP3–SEP3ΔC heterodimer should be observed when both are applied together. Figure 1A shows that one intermediate shift can indeed be observed (band '2b'), indicating that SEP3 binds as a dimer to a DNA fragment carrying one CArG box. However, when a probe carrying two CArG boxes is used, five additional complexes (Figure 1A, bands '4a–4e') can be resolved when full-length and C-terminal deleted SEP3 are mixed. This is likely caused by the binding of four SEP3 proteins to this DNA fragment (Figure 1A). However, in these assays it cannot be distinguished whether two dimers bind independently to the two CArG boxes, or whether a tetramer binds to both CArG boxes by looping the intervening DNA (Figure 1B). A striking feature of protein complexes that loop DNA is cooperativity in protein-DNA assembly (48). Additional EMSAs were therefore performed to examine whether SEP3 binds cooperatively to DNA.

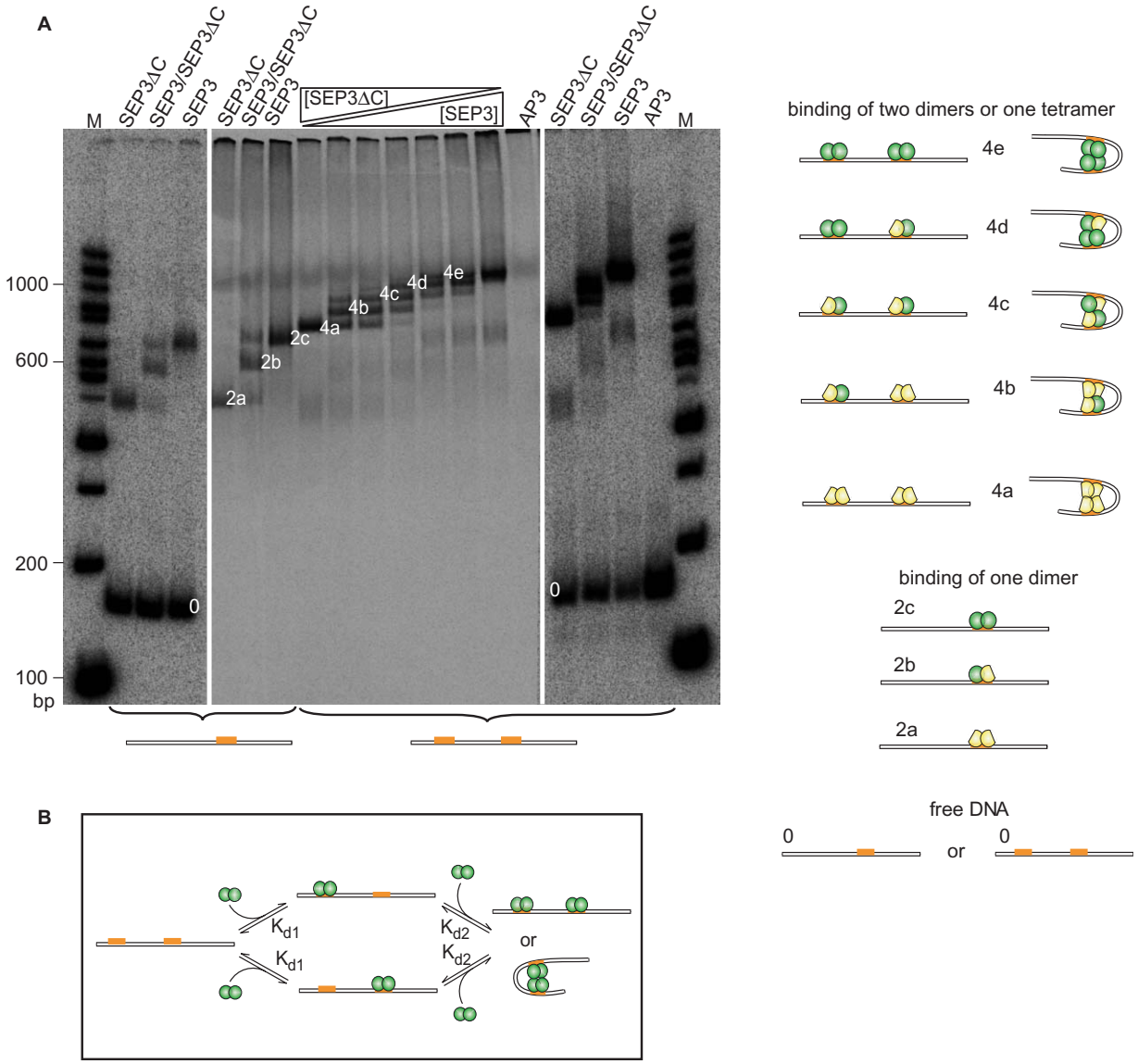

Figure 1. Stoichiometry of SEP3 protein–DNA assembly. (**A**) EMSA in which full length ('SEP3') and C-terminal deleted SEP3 ('SEP3ΔC') were co-incubated at different ratios obtained by mixing plasmid templates in ratios of 0:1, 1:5, 1:3, 1:1, 3:1, 5:1 or 1:0. Per reaction, 2 µl of *in vitro* translated protein was used. DNA fragments carried either one or two CArG boxes (orange bars) as depicted at the bottom of the gel. Proteins applied are noted above the gel. AP3, that alone is not expected to bind to DNA, was used as a negative control. In lanes where no free DNA (marked by '0') is visible, proteins were labelled instead of DNA for the sake of band resolution. Signals obtained with radioactively labelled DNA are shown on the right and on the left for comparison. Bands are marked with numbers ('0', '2' and '4') according to the number of proteins bound to the DNA fragment; lowercase letters are used to differentiate between complexes composed of different proteins. The inferred complex composition is shown on the right. Full length proteins are shown in green, truncated ones in yellow. 'M' denotes marker lanes in which a radioactively labelled DNA ladder (100-bp DNA ladder, NEB) was applied. All signals were obtained from a single gel, but exposure time for lanes containing radioactively labelled DNA fragments was different from the rest. (**B**) Proposed mechanism of MADS domain protein–DNA assembly. Binding of the first protein dimer to a CArG box is characterized by the dissociation constant K_{d1}, binding of the second dimer is characterized by the dissociation constant K_{d2}. Binding of the second dimer can be independent of binding of the first dimer, or cooperative and involving DNA looping.

Cooperativity in a two-site system is best examined if both binding sites are bound with equal affinity (29). In order to meet this criterion, we used a suitably designed DNA fragment containing the same CArG box twice. To ensure that binding affinity to these sites is the same, we calculated binding isotherms from EMSAs with probes in which either of the two CArG boxes was replaced by a randomized sequence of the same nucleotide composition (Supplementary Figure S1). Both isotherms were nearly identical, thus confirming equal affinity of binding to both CArG boxes (Supplementary Figure S1).

For measuring cooperativity, increasing amounts of *in vitro* translated protein were incubated with a DNA fragment carrying two CArG boxes that are spaced by six helical turns (assuming 10.5 bp per helical turn, i.e. 63 bp, as measured from CArG box centre to CArG box centre). Surprisingly, a complex consisting of four SEP3 proteins was readily detected while only a small

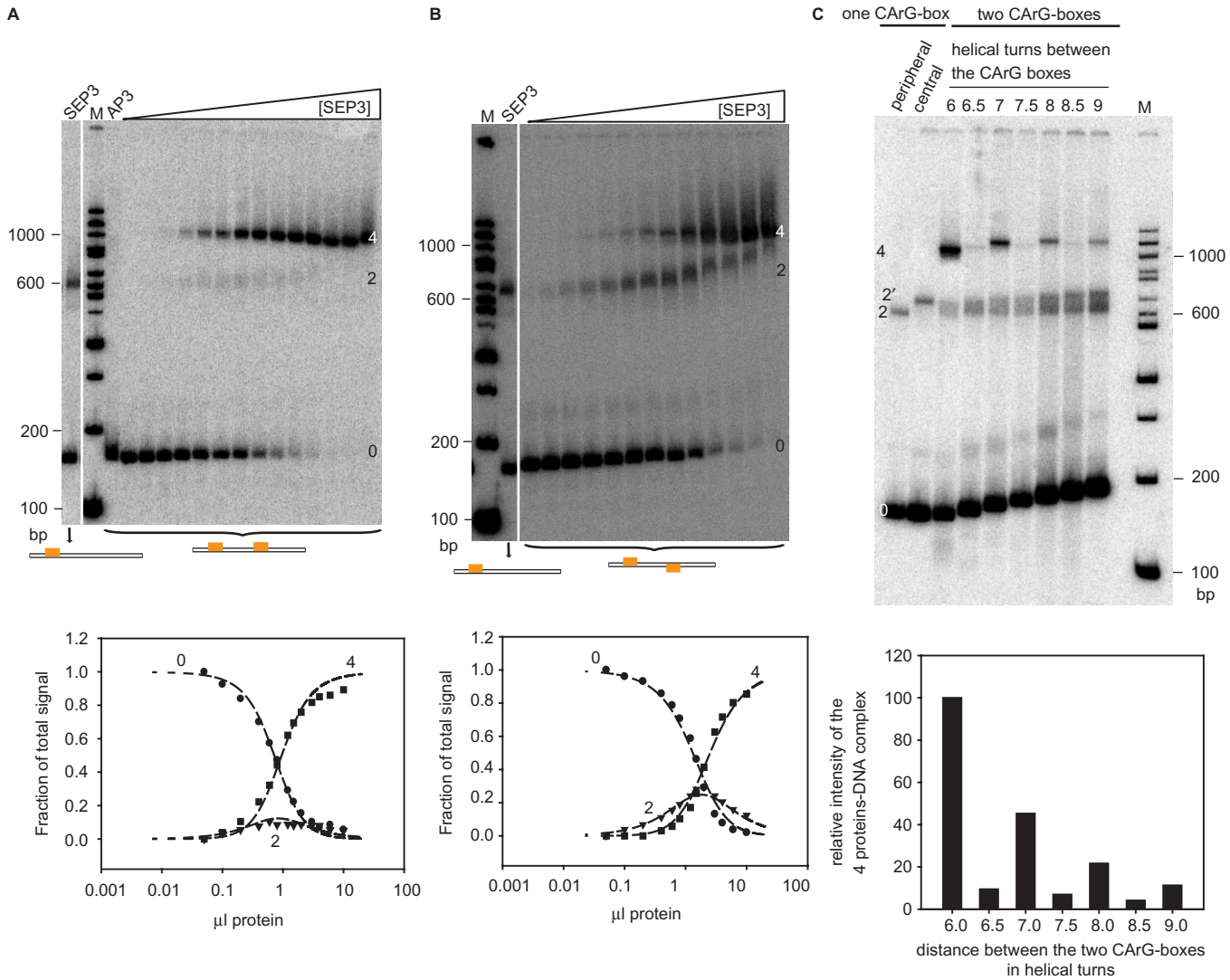

Figure 2. Analysis of cooperative DNA binding of SEP3. (**A** and **B**) Examples of EMSAs used to determine cooperative DNA binding of SEP3. Different protein concentrations were added to a DNA probe carrying two CArG boxes. (A) A DNA probe carrying two CArG boxes spaced by 6 helical turns was used. (B) Spacing between the CArG boxes was 6.5 helical turns. Comparing the gel pictures shown in (A) and (B), the difference in cooperative binding is evident by the stronger signal caused by a DNA-bound SEP3 dimer ('2') in (B). (DNA fragments to which a single SEP3 dimer is bound migrate more slowly at increased protein concentration possibly due to higher glycerol concentrations in these samples.) For size comparison, a SEP3 dimer bound to a probe containing only one CArG box is shown always on the left. Quantitative analysis showing the fractional saturation of the different bands (circles: free DNA; triangles: one dimer bound; squares: two dimer/tetramer bound) is shown below each gel picture. Binding curves were calculated as described in Materials and methods section. (**C**) Phase dependence of the formation of the SEP3–DNA complex. The binding cocktail contained 0.4 µl of *in vitro* translated protein. Signals resulting from complexes bound to probes containing one CArG box are shown in the leftmost lanes. A dimer bound to a CArG box peripheral located on the DNA fragment is indicated by '2', whereas '2'' indicates a dimer bound to a CArG box centrally located on the DNA fragment. The difference in migration of the two complexes results in part from the ability of SEP3 to bend DNA. Below the gel picture, quantitative analysis of homotetramer formation is shown. Fractional saturation of the signal intensity caused by the homotetramer is expressed as percentage of the fractional saturation of the homotetramer bound to the CArG boxes spaced by 6 helical turns. Band assignment is as in Figure 1.

fraction of DNA was bound by a single SEP3 dimer (Figure 2A). In these experiments, single SEP3 dimers did bind <20% of the total DNA per lane, a clear hallmark of a cooperative protein–DNA interaction (29,49). Quantitative analysis of the signals indicated that the relative dissociation constant for binding of a SEP3 dimer to the CArG box is around 80-fold decreased when one dimer is already bound to the neighbouring CArG box (Table 1).

In general, computational and experimental analyses indicate that—if the protein–DNA interactions are weak—the observed pattern can also be obtained for a completely non-cooperative system (50). This is because singly bound complexes tend to dissociate more easily than doubly bound complexes during gel run and hence give unrepresentative weak signals (50). To study whether considerable complex dissociation occurs during gel run, we analysed binding of SEP3 to a DNA fragment

Table 1. Domain structure of SEP3 [positions where SEP3ΔC and SEP3ΔK3C have been truncated are indicated (amino acid positions in brackets)] and apparent K_{d1}/K_{d2} ratios determined for the different proteins binding to probes containing two CArG boxes spaced by 6 or 6.5 helical turns

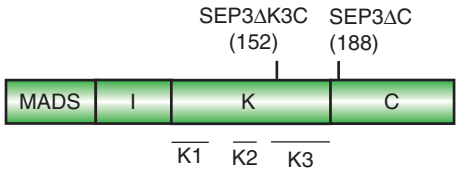

CArG boxes separated by 6 helical turns		CArG boxes separated by 6.5 helical turns	
K_{d1}/K_{d2}		K_{d1}/K_{d2}	
SEP3	83 (±15)	SEP3	10 (±0.8)
SEP3ΔC	89 (±34)	SEP3ΔC	9.6 (±1)
SEP3ΔK3C	3.2 (±0.5)	SEP3ΔK3C	3.5 (±0.2)

The K_{d1}/K_{d2} ratios represent the mean of at least three independent experiments; standard errors are given in brackets.

containing one CArG box. It is assumed that the disappearance of free DNA is independent of complex dissociation and thus a more reliable estimator of binding strength (51). Independent analysis of binding curves obtained for bound and unbound DNA fragments should thus yield similar K_d values if no complex dissociation occurs (29). With our experimental setup, we estimated that K_d values differed around 2.5-fold or less when analysing bound and unbound fragments separately (Supplementary Figure S1). This indicates that only little complex dissociation occurs during gel run and that the attenuation of the dimer band observed when a fragment carrying two CArG boxes is incubated together with SEP3 is indeed largely due to cooperative binding.

Cooperative binding of SEP3 is phase-dependent and involves DNA loop formation

Cooperative binding of proteins to two distant DNA sites can in principle be achieved by at least two mechanisms. Cooperativity can result from alterations in DNA structure after protein binding to one site that in turn facilitates binding to the second site. Alternatively, cooperativity is mediated by direct protein–protein interactions between the proteins bound to the two sites, requiring DNA looping when the distance between the DNA sites is greater than the radius of the proteins.

To distinguish between these possibilities in case of SEP3 binding to CArG boxes, we employed the fact that cooperative protein–DNA interactions are expected to critically depend on the stereo-specific alignment of the respective *cis*-regulatory DNA elements in case direct protein–protein interactions are involved (48,52). In the experiments shown in Figure 2A, the CArG boxes were spaced by 6 helical turns (63 bp). Hence, SEP3 dimers bound to the two CArG boxes are expected to directly face each other. In contrast, increasing the spacing from 6 to 6.5 helical turns rotates one site with respect to the other half a turn around the helical axis. Loop formation would now require twisting the DNA so that the two sites face each other again. This is energetically costly and decreases the frequency of loop formation (48,52,53).

Indeed, cooperativity significantly dropped when the spacing between the CArG boxes was increased from 6 to 6.5 helical turns (68 bp) by inserting five nucleotides in the intervening region (Figure 2B, Table 1). Cooperativity was to a large extent re-established, however, when the distance between the CArG boxes was increased to 7 helical turns (74 bp) (Figure 2C). In general, this stereo-specificity in binding was confirmed for distances between the CArG boxes from 6 to 9 helical turns in increments of half helical turns (Figure 2C). These data strongly suggest that a quartet of SEP3 proteins binds cooperatively to two appropriately oriented *cis*-regulatory DNA elements by looping the intervening DNA.

Further evidence that a SEP3 tetramer binds to its target sites by DNA looping is provided by DNase I footprint analyses. As DNase I preferentially cuts sequences located in widened minor grooves and hence is sensitive to structural changes of the DNA, footprints have successfully been used to show DNA looping upon protein binding (48,52). Probing a complex consisting of four SEP3 proteins bound to DNA with DNase I yielded a digestion pattern that resembles that observed for other cases of protein-induced DNA loops (48,52). The two CArG boxes are protected, while the intervening region shows a characteristic pattern with sites of enhanced and diminished DNase I sensitivity. Sites of similar differential sensitivity are spaced in ~10-bp intervals, so that they all come to lie on one side of the DNA helix (Figure 3). This supports our conclusion that SEP3 homotetramers loop DNA upon binding to two distant CArG boxes.

Deletion of the K3 subdomain impairs cooperative binding and looping of DNA

Floral homeotic MADS domain proteins have a modular structure, comprising the DNA-binding MADS domain followed by the intervening- (I-), keratin-like (K-) and C-terminal domain (Table 1) (54–57). The K domain and the C-terminal domain are thought to be involved in mediating protein–protein interactions (58). We used two truncated versions of the SEP3 protein to study which domains are required for tetramerization of SEP3 upon DNA binding. As described above, in SEP3ΔC almost the whole C-terminal domain [as defined in Ref. (55)] is deleted, while SEP3ΔK3C also lacks K3, a subdomain of the K domain (Table 1). The EMSAs and BiFCs, respectively, indicated that both of the truncated versions are capable of binding to DNA as dimers *in vitro*, as well as of dimerization and nuclear translocation *in planta* (Figures 4 and 5). However, while SEP3ΔC is indistinguishable from the full-length protein in terms of cooperative DNA binding, SEP3ΔK3C shows a clear reduction in cooperativity (Figure 4A and B, Table 1). Also, stereo-specific DNA-binding was observed for SEP3ΔC, but not for SEP3ΔK3C (Figure 4).

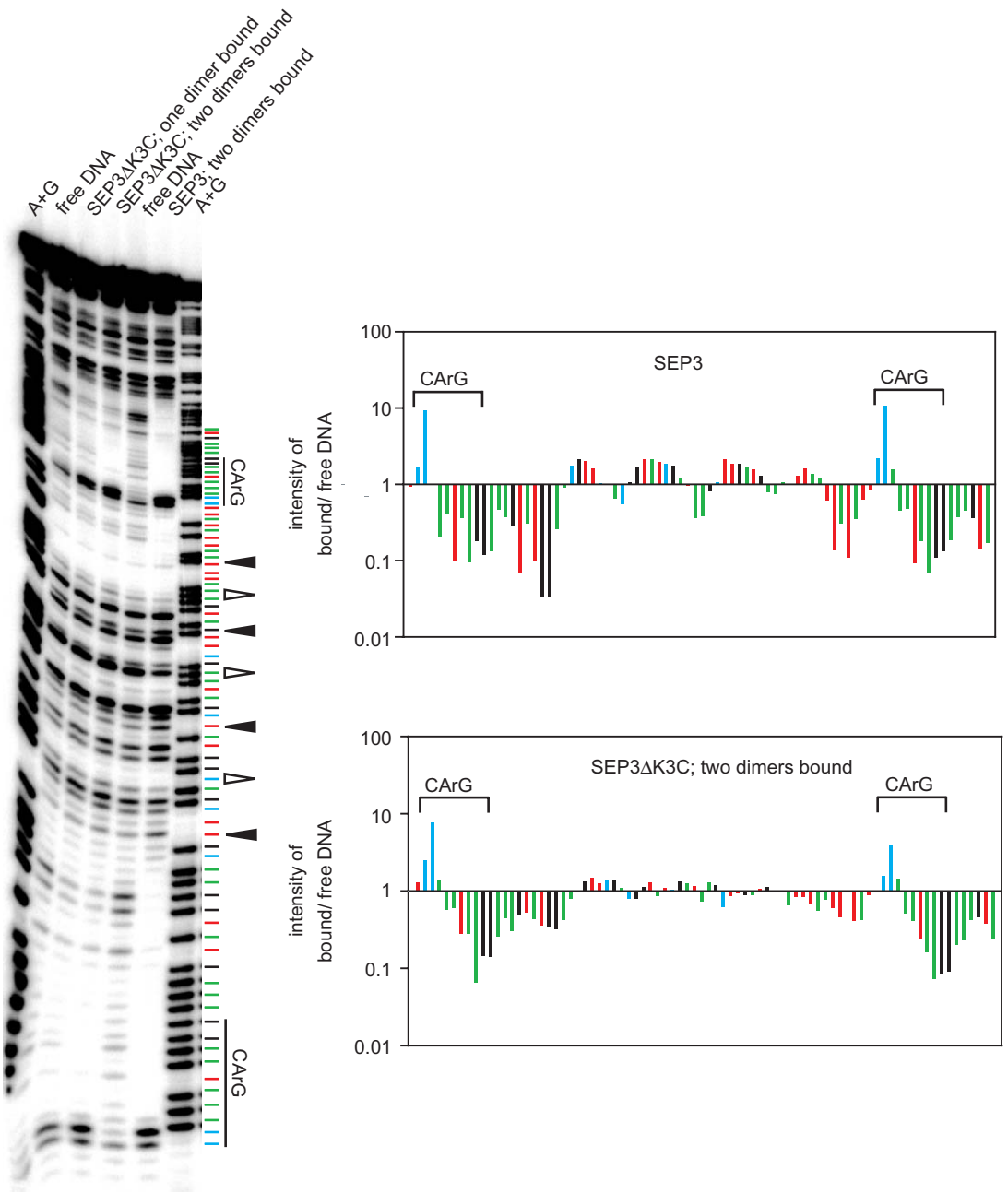

Figure 3. DNase I footprint assays. SEP3 or SEP3ΔK3C was incubated with a DNA probe carrying two CArG boxes spaced by 6 helical turns. For SEP3ΔK3C, but not for SEP3, a complex with one dimer bound could be obtained at sufficient signal intensity and thus was also analysed on the sequencing gel. Protein–DNA complexes analysed are noted above the gel. An A + G sequencing reaction of the DNA probe used is shown for comparison. Sequence of the DNA is depicted on the right (blue = cytosine, red = thymine, green = adenine, black = guanine); the position of the CArG boxes is indicated. Open and filled arrowheads point towards sites of diminished and enhanced DNase I sensitivity, respectively. On the right, quantitative analysis of the gel picture shows the change of sensitivity to DNase I digestion after protein binding, in single base pair steps, using free DNA as a reference after correction for differences in DNA-loading by using invariable bands as an internal standard. The region protected by full-length SEP3 extends beyond the CArG boxes, probably because these DNA regions are in close contact to the protein surface in the looped complex.

In addition, sites of enhanced and diminished sensitivity in DNase I footprints, as observed for SEP3, were not observed for SEP3ΔK3C (Figure 3).

Many MADS domain proteins show the capability to bend DNA. This could, in principle, facilitate loop formation. We therefore determined the bending angles induced by SEP3 and SEP3ΔK3C using circular permutation analysis. Bending was not severely impaired in SEP3ΔK3C, with distortion angles of around 51° and 57° for SEP3 and SEP3ΔK3C, respectively (Figure 6).

DISCUSSION

Here we provide data strongly suggesting that four molecules of the class E floral homeotic protein SEP3 bind

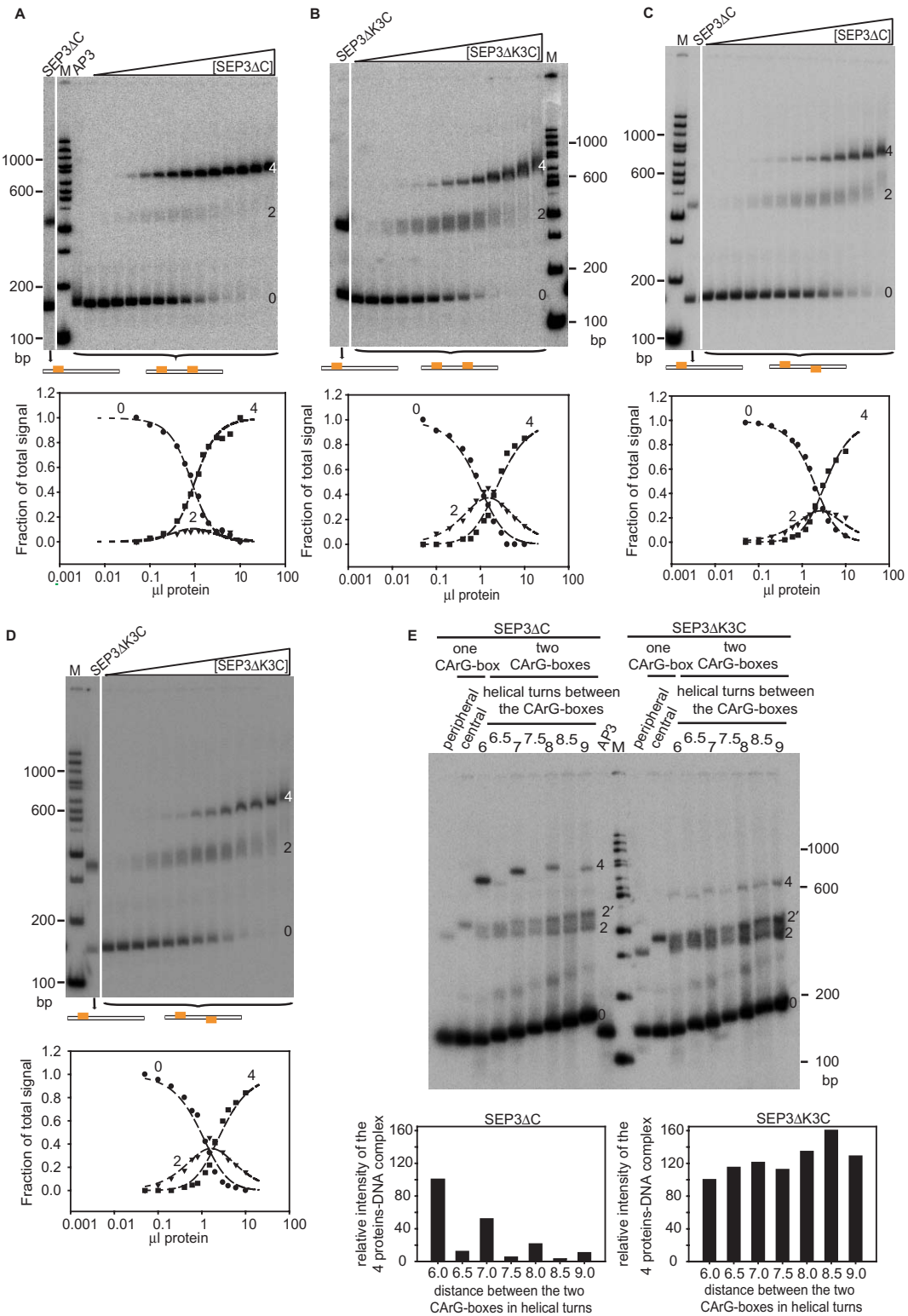

Figure 4. Examples of EMSAs used to determine cooperativity of DNA binding of SEP3ΔC and SEP3ΔK3C. (**A–D**) show EMSAs in which increasing amounts of SEP3ΔC (A and C) or SEP3ΔK3C (B and D) were incubated with DNA probes carrying two CArG-boxes spaced by 6 (A and B) or 6.5 (C and D) helical turns. As in Figure 2, quantitative analysis of the band pattern is shown below each gel picture. The ability of the proteins to bind as dimers to a DNA fragment carrying one CArG box is shown in the leftmost lanes of (A) and (B). (**E**) Analysis of the phasing of two CArG boxes on the formation of a SEP3ΔC–DNA and SEP3ΔK3C–DNA complex. 0.4 µl of *in vitro* translated protein was used. Signals resulting from complexes bound to probes containing one CArG box are shown in the leftmost lanes. A dimer bound to a CArG box peripheral located on the DNA fragment is indicated by '2', whereas '2′' indicates a dimer bound to a CArG box centrally located on the DNA fragment. As both, SEP3ΔC and SEP3ΔK3C, bend DNA, the differential positioning of the CArG box on the fragment results in a difference in migration of the complexes (2 and 2′). As in Figure 2C, quantitative analysis of the complex consisting of four proteins bound to DNA is shown below the gel picture.

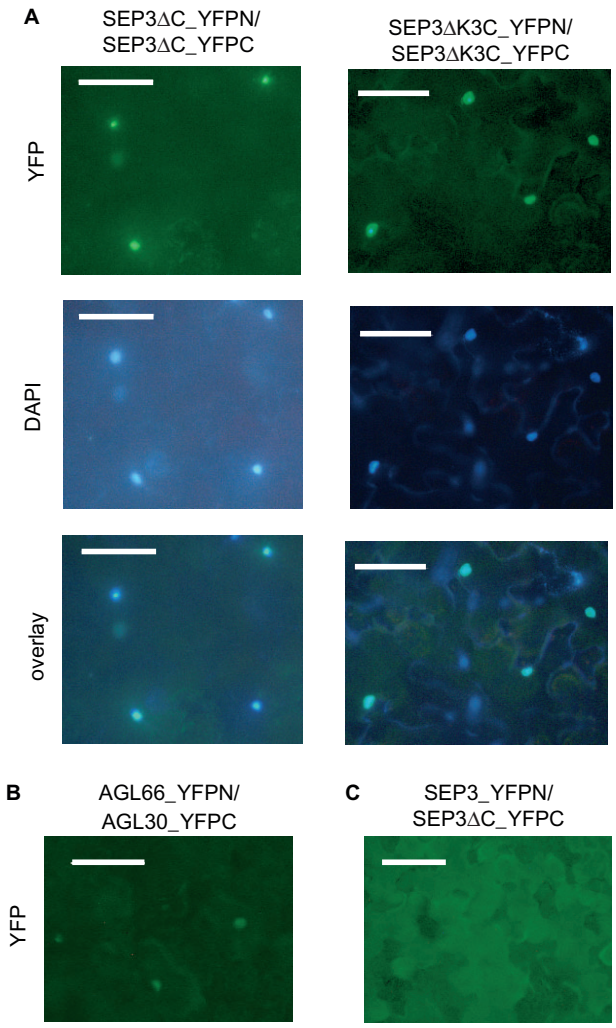

Figure 5. (**A**) Subcellular localization and *in planta* dimerization of SEP3ΔC and SEP3ΔK3C. Proteins are expressed as fusions with the N- (YFPN) or C-terminal (YFPC) part of YFP as indicated above the picture in *Nicotiana benthamiana* leaves. Leaf sections were analysed with a fluorescence microscope. YFP signals are shown in the upper row, nuclear staining using DAPI is shown in the middle row. The overlay in the lower row shows co-localization of the DAPI and YFP signals. (**B**) The YFP signals of two proteins known to interact, i.e. AGL30 (fused to the C-terminal part of YFP) and AGL66 (fused to the N-terminal part of YFP) is shown as a positive control. (**C**) No YFP signal could reliably be detected when full-length SEP3 was tested alone or in combination with a C-terminal deleted version, as exemplarily shown for SEP3 (fused to the N-terminal part of YFP) co-expressed with SEP3ΔC (fused to the C-terminal part of YFP). This might be due to steric hindrance of the C-terminal domain. Scale bars, 100 µm.

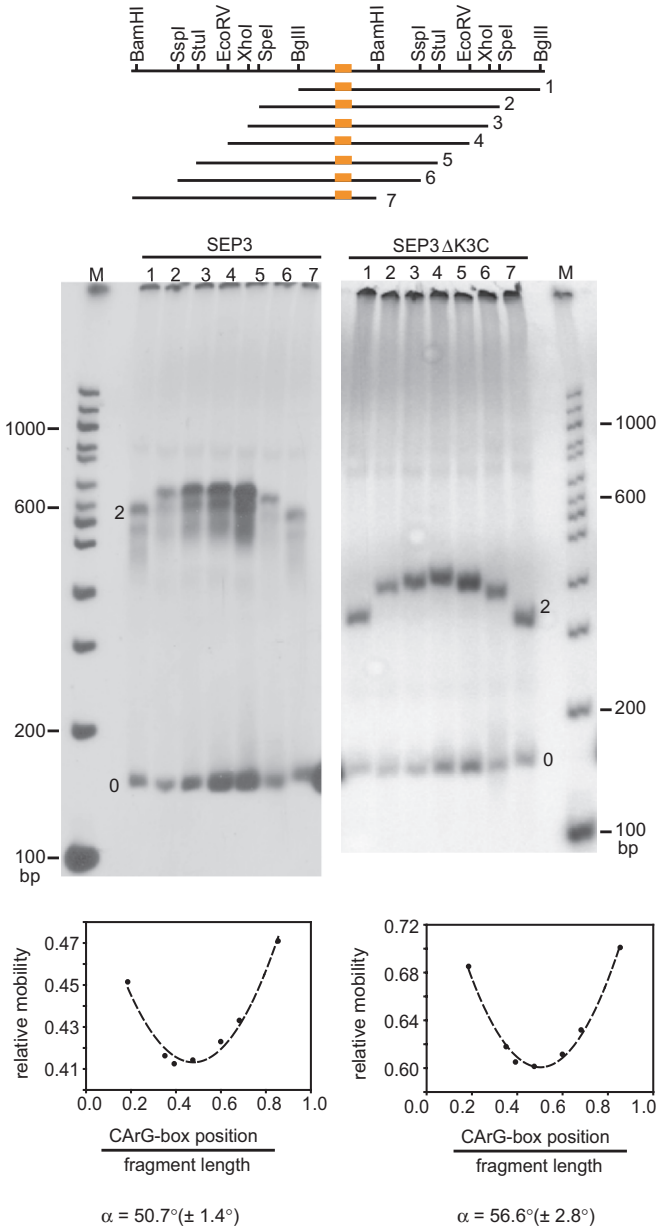

Figure 6. Circular permutation analysis of DNA distortions induced by SEP3 and SEP3ΔK3C. The gel picture shows EMSAs with SEP3 and SEP3ΔK3C bound to circularly permutated probes. *In vitro* translated SEP3 and SEP3ΔK3C of 4 µl and 2 µl, respectively, were used. DNA probes and restriction endonucleases used to prepare them are schematically depicted above the gel. The CArG box is indicated by an orange bar. In the diagram below the gel, the complex mobility is plotted against the relative position of the CArG boxes. Bending angles represent the means of at least four different experiments (standard error in brackets). Band assignment is as in Figure 1.

cooperatively to DNA fragments carrying two CArG boxes by looping the intervening DNA. This shows that SEP3 has the intrinsic ability to constitute quartet complexes and to generate protein-induced DNA loops, as has also been predicted for floral quartets.

Loop formation and target gene specificity

In our experimental setup, the accurate stereo-specific alignment of the CArG boxes was an essential prerequisite for cooperative binding of SEP3. We also found that the formation of tetrameric complexes declines with increasing distance between the CArG boxes (Figure 2C). This is in line with theoretical studies predicting that the probability of loop formation is highest when the span of the protein complex is similar to the contour length of the DNA and decreases rapidly with an increased distance between the binding sites (59). This is interpreted to be the result of the low elastic bending energy required to

bring the protein dimers together over these short distances; the energy increases with higher distances between the binding sites (59) and thus results in lower looping probabilities. Also, the ability of SEP3 to bend DNA at the binding site (CArG box) might, although to a minor extent, affect the optimal size of a DNA loop and thus could at least partly be responsible for the decline of complex formation with increasing distance between the CArG boxes.

Precedent cases from other eukaryotic systems suggest that the phasing and spacing of cis-regulatory binding sites is also of relevance *in vivo* (60–63). Furthermore, given the close relationship of floral homeotic MADS domain proteins, we are confident that the phase- and distance-dependent DNA binding of SEP3 homotetramers serves as a general model of how floral homeotic protein complexes interact with DNA. If so, it would set constraints on the arrangement of CArG boxes in target gene promoters and hence may be an important factor of how target gene specificity is achieved. Indeed, in some target gene promoters of MADS domain proteins, CArG boxes are clustered as in our experiments; for example, two of the three CArG boxes in the *GLO* promoter of *A. majus* are spaced by 5.1 helical turns (54 bp), two of the three CArG boxes in the *AP3* promoter are spaced by 7 helical turns (73 bp) and the two CArG boxes in the *CRABS CLAW* promoter are spaced by 8.2 helical turns (86 bp) (41,64–66). There is evidence that these CArG boxes are indeed bound by MADS-type floral homeotic proteins *in planta* (41,65–67).

However, besides these relatively small DNA loops, it is conceivable that much bigger MADS domain protein-induced DNA loops are formed *in vivo*, and that factors not considered here, such as nucleosomes (chromatin structure), might influence the formation of floral quartets. In line with this, the two CArG boxes in *GA4*, a target gene of *AGAMOUS*, are spaced 1500 bp from each other (67). It thus remains a goal for future research to study the relevance of the positioning of CArG boxes to each other *in vivo*, for example by transgenic reporter gene assays in which the distance between two CArG boxes is systematically varied. Moreover, whether a promoter region involving two or more CArG boxes has a looped DNA conformation *in vivo* could be determined employing chromosome conformation capture or a related technique (68,69).

On the biological significance of SEP3 homotetramers

Whether SEP3 functions only in heteromeric complexes such as those described by the floral quartet model, or whether also homotetramers of SEP3 have a function *in planta* is not clear so far. Even though there is no conclusive evidence that *SEP3* has any function independent of other MADS box genes, the available data certainly also do not exclude such a function. As detailed above, *SEP3* is in several respects functionally distinct from the other *SEP* genes; it is thus quite conceivable that SEP3 homotetramers might be of biological relevance at some stage and/or in certain tissues during flower development.

One function could be in increasing developmental robustness. Using plants ectopically expressing *SEP3* under control of the CaMV 35S promoter (35S::*SEP3*), it was shown that *SEP3* is sufficient to activate class B and class C floral homeotic genes in leaves (23). Although SEP3 is usually not required for the initial activation of class B and class C floral homeotic genes, as these are normally expressed in *sep1 sep2 sep3* triple mutants (13), a redundant and normally masked function of SEP3 in the activation of floral homeotic genes might increase the robustness of a critical developmental process, i.e. flower formation. At stage 1 of floral development in *A. thaliana*, the class A gene *AP1*, among others, is activated by *LEAFY* (70–72). Afterwards, *SEP3* is activated at stage 2 (13,73), so that AP1 and SEP3 can now interact to promote floral meristem identity (23,24), probably by activating the floral organ identity genes, *AP3*, *PI* and *AG*, at stage 3 in parallel to the activation by *LEAFY*. It is conceivable, therefore, that SEP3 tetramers provide a redundant means of floral homeotic gene activation that becomes of critical importance when, during development, other factors such as LEAFY are not available at a sufficient concentration, for example because of stochastic events during gene expression.

However, even if SEP3 homotetramers do not have a function *in planta*, we find it likely that the ability of SEP3 to bind cooperatively to DNA by DNA looping could be of considerable importance for floral quartet formation. SEP proteins are involved in many processes during flower development, and they might serve as molecular bridges that integrate other floral homeotic proteins in quartet complexes. Along these lines, the ability of SEP3 to bind cooperatively to DNA might be of importance. In general, cooperative DNA binding of transcription factors is regarded to be of high relevance in many developmental processes. For the BICOID protein from *Drosophila*, for example, cooperative binding is essential for establishing sharp expression boundaries of some target genes and hence for the morphogenic function of BICOID (74). It has therefore been proposed that cooperative DNA binding is crucial for transcription factors to act as developmental switches (75). The angiosperm flower is a highly compressed structure in which different floral organs have to be specified reliably in tight vicinity to each other in a temporally controlled manner. We thus hypothesize that cooperative binding—conferred to quartet-like complexes by SEP proteins—constitutes essential developmental switches during flower development.

Role of the K3 subdomain in higher order complex formation

We have shown that deletion of the C-terminal domain does not impair cooperative DNA binding of SEP3, while additional truncation of subdomain K3 leads to a clear reduction in cooperativity (Figure 4, Table 1). This indicates that the domains M, I and K are sufficient for cooperative DNA binding of SEP3, and that K3 is required for cooperative DNA binding, at least in the absence of the C-terminal domain. Whether the C-terminal domain could substitute for K3 in terms of cooperative binding remains

to be tested using internal deletion constructs in which K3, but not the C-terminal domain, is removed.

The K3 subdomain is predicted to form an amphipathic α-helix (55,76). Neither dimerization nor DNA bending is severely affected in the K3-deleted version of SEP3 (Figures 4–6). For SEP1, as well as for other floral homeotic proteins, it has been demonstrated that the K3 subdomain is not involved in DNA binding (44,77,78). Rather, it has been suggested that K3 is involved in mediating protein–protein interactions between floral homeotic proteins [Ref. (58) and references therein]. Taken together, these data support our conclusion that two DNA-bound SEP3 dimers can undergo direct protein–protein interactions, and that the K3 subdomain is directly involved in mediating protein–protein interactions between the dimers, but not in DNA bending or in protein–protein interactions between SEP3 monomers.

We are just beginning to elucidate the chemical and physical details of MADS domain protein interactions with DNA. Future research will tell us how representative our findings with SEP3 are for floral homeotic proteins in general. This again will help us to better understand developmental switches during flower development at the molecular level.

SUPPLEMENTARY DATA

Supplementary Data are available at NAR Online.

ACKNOWLEDGEMENTS

It is a pleasure to acknowledge the excellent technical assistance of Ulrike Wrazidlo and Jana Hrtoňová. We are also grateful to Markus Ritz for help with data analysis and to Gerhard Steger (University of Düsseldorf) and Thomas P. Jack (Dartmouth College, Hanover) for helpful comments on an earlier version of this article. Thanks to Joachim Uhrig (University of Cologne) and Sankar Adhya (National Institutes of Health, Bethesda) for providing the pBaTL and pBEND2 vectors, respectively. We are grateful to Heinz Saedler and Thomas Münster (Max Planck Institute for Plant Breeding Research, Cologne) for their support with the BiFC experiments, and to the group of Jürgen Kroymann (Max Planck Institue for Chemical Ecology, Jena) for support with the phosphorimager analyses. We thank Kerstin Kaufmann for support during initial stages of this project. Special thanks to Domenica Schnabelrauch (Max Planck Institute for Chemical Ecology, Jena) for all her sequencing efforts. Many thanks also to the Friedrich Schiller University Jena for general support. G.T. thanks Casper for flashes of inspiration.

FUNDING

Studienstiftung des deutschen Volkes (to R.M.); Deutsche Forschungsgemeinschaft (DFG, TH 417/5-1 and 2 to G.T.). Funding for open access charge: Deutsche Forschungsgemeinschaft (TH 417/5-1 and 2).

Conflict of interest statement. None declared.

REFERENCES

1. Hughes,C.L. and Kaufman,T.C. (2002) Hox genes and the evolution of the arthropod body plan. *Evol. Dev.*, **4**, 459–499.
2. Veraksa,A., Del Campo,M. and McGinnis,W. (2000) Developmental patterning genes and their conserved functions: from model organisms to humans. *Mol. Genet. Metabol.*, **69**, 85–100.
3. Haughn,G.W. and Somerville,C.R. (1988) Genetic control of morphogenesis in *Arabidopsis*. *Dev. Genet.*, **9**, 73–89.
4. Coen,E.S. and Meyerowitz,E.M. (1991) The war of the whorls - genetic interactions controlling flower development. *Nature*, **353**, 31–37.
5. Mandel,M.A., Gustafson-Brown,C., Savidge,B. and Yanofsky,M.F. (1992) Molecular characterization of the *Arabidopsis* floral homeotic gene *APETALA1*. *Nature*, **360**, 273–277.
6. Yanofsky,M.F., Ma,H., Bowman,J.L., Drews,G.N., Feldmann,K.A. and Meyerowitz,E.M. (1990) The protein encoded by the *Arabidopsis* homeotic gene *AGAMOUS* resembles transcription factors. *Nature*, **346**, 35–39.
7. Jack,T., Brockman,L.L. and Meyerowitz,E.M. (1992) The homeotic gene *APETALA3* of *Arabidopsis thaliana* encodes a MADS box and is expressed in petals and stamens. *Cell*, **68**, 683–697.
8. Jofuku,K.D., den Boer,B.G.W., Van Montagu,M. and Okamuro,J.K. (1994) Control of *Arabidopsis* flower and seed development by the homeotic gene *APETALA2*. *Plant Cell*, **6**, 1211–1225.
9. Goto,K. and Meyerowitz,E.M. (1994) Function and regulation of the *Arabidopsis* floral homeotic gene *PISTILLATA*. *Gene Dev.*, **8**, 1548–1560.
10. Krizek,B.A. and Meyerowitz,E.M. (1996) The *Arabidopsis* homeotic genes *APETALA3* and *PISTILLATA* are sufficient to provide the B class organ identity function. *Development*, **122**, 11–22.
11. Mizukami,Y. and Ma,H. (1992) Ectopic expression of the floral homeotic gene *AGAMOUS* in transgenic *Arabidopsis* plants alters floral organ identity. *Cell*, **71**, 119–131.
12. Mandel,M.A. and Yanofsky,M.F. (1995) A gene triggering flower formation in *Arabidopsis*. *Nature*, **377**, 522–524.
13. Pelaz,S., Ditta,G.S., Baumann,E., Wisman,E. and Yanofsky,M.F. (2000) B and C floral organ identity functions require *SEPALLATA* MADS-box genes. *Nature*, **405**, 200–203.
14. Ditta,G., Pinyopich,A., Robles,P., Pelaz,S. and Yanofsky,M.F. (2004) The *SEP4* gene of Arabidopsis thaliana functions in floral organ and meristem identity. *Curr. Biol.*, **14**, 1935–1940.
15. Theißen,G. (2001) Development of floral organ identity: stories from the MADS house. *Curr. Opin. Plant Biol.*, **4**, 75–85.
16. Honma,T. and Goto,K. (2001) Complexes of MADS-box proteins are sufficient to convert leaves into floral organs. *Nature*, **409**, 525–529.
17. Pelaz,S., Tapia-Lopez,R., Alvarez-Buylla,E.R. and Yanofsky,M.F. (2001) Conversion of leaves into petals in Arabidopsis. *Curr. Biol.*, **11**, 182–184.
18. Egea-Cortines,M., Saedler,H. and Sommer,H. (1999) Ternary complex formation between the MADS-box proteins SQUAMOSA, DEFICIENS and GLOBOSA is involved in the control of floral architecture in *Antirrhinum majus*. *EMBO J.*, **18**, 5370–5379.
19. Theißen,G. and Saedler,H. (2001) Plant biology. Floral quartets. *Nature*, **409**, 469–471.
20. Krizek,B.A. and Fletcher,J.C. (2005) Molecular mechanisms of flower development: an armchair guide. *Nat. Rev. Genet.*, **6**, 688–698.
21. Favaro,R., Pinyopich,A., Battaglia,R., Kooiker,M., Borghi,L., Ditta,G., Yanofsky,M.F., Kater,M.M. and Colombo,L. (2003) MADS-box protein complexes control carpel and ovule development in *Arabidopsis*. *Plant Cell*, **15**, 2603–2611.
22. Kaufmann,K., Anfang,N., Saedler,H. and Theissen,G. (2005) Mutant analysis, protein-protein interactions and subcellular localization of the Arabidopsis B-sister (ABS) protein. *Mol. Genet. Genomics*, **274**, 103–118.
23. Castillejo,C., Romera-Branchat,M. and Pelaz,S. (2005) A new role of the *Arabidopsis SEPALLATA3* gene revealed by its constitutive expression. *Plant J.*, **43**, 586–596.
24. Pelaz,S., Gustafson-Brown,C., Kohalmi,S.E., Crosby,W.L. and Yanofsky,M.F. (2001) APETALA1 and SEPALLATA3 interact to promote flower development. *Plant J.*, **26**, 385–394.

25. Zahn,L.M., King,H.Z., Leebens-Mack,J.H., Kim,S., Soltis,P.S., Landherr,L.L., Soltis,D.E., dePamphilis,C.W. and Ma,H. (2005) The evolution of the SEPALLATA subfamily of MADS-Box genes: a preangiosperm origin with multiple duplications throughout angiosperm history. *Genetics*, **169**, 2209–2223.
26. Jack,T. (2004) Molecular and genetic mechanisms of floral control. *Plant Cell*, **16**, S1–S17.
27. Jack,T. (2001) Relearning our ABCs: new twists on an old model. *Trends Plant Sci.*, **6**, 310–316.
28. Sambrook,J. and Russell,D.W. (2001) *Molecular Cloning: A Laboratory Manual*, 3rd edn. Cold Spring Harbor Laboratory Press, Cold Spring Harbor.
29. Senear,D.F. and Brenowitz,M. (1991) Determination of binding constants for cooperative site-specific protein-DNA interactions using the gel mobility-shift assay. *J. Biol. Chem.*, **266**, 13661–13671.
30. Steger,G. (2005) *Bioinformatik. Methoden zur Vorhersage von RNA- und Proteinstruktur*. Birkhäuser Verlag, Basel.
31. Riechmann,J.L., Wang,M.Q. and Meyerowitz,E.M. (1996) DNA-binding properties of *Arabidopsis* MADS domain homeotic proteins APETALA1, APETALA3, PISTILLATA and AGAMOUS. *Nucleic Acids Res.*, **24**, 3134–3141.
32. Kim,J., Zwieb,C., Wu,C. and Adhya,S. (1989) Bending of DNA by gene-regulatory proteins: construction and use of a DNA bending vector. *Gene*, **85**, 15–23.
33. Rasko,T., Finta,C. and Kiss,A. (2000) DNA bending induced by DNA (cytosine-5) methyltransferases. *Nucleic Acids Res.*, **28**, 3083–3091.
34. Nagaich,A.K., Appella,E. and Harrington,R.E. (1997) DNA bending is essential for the site-specific recognition of DNA response elements by the DNA binding domain of the tumor suppressor protein p53. *J. Biol. Chem.*, **272**, 14842–14849.
35. Ferrari,S., Harley,V.R., Pontiggia,A., Goodfellow,P.N., Lovell-Badge,R. and Bianchi,M.E. (1992) SRY, like HMG1, recognizes sharp angles in DNA. *EMBO J.*, **11**, 4497–4506.
36. Verelst,W., Saedler,H. and Münster,T. (2007) MIKC* MADS-protein complexes bind motifs enriched in the proximal region of late pollen-specific *Arabidopsis* promoters. *Plant Physiol.*, **143**, 447–460.
37. Bracha-Drori,K., Shichrur,K., Katz,A., Oliva,M., Angelovici,R., Yalovsky,S. and Ohad,N. (2004) Detection of protein-protein interactions in plants using bimolecular fluorescence complementation. *Plant J.*, **40**, 419–427.
38. Bencini,D., O'Donovan,G. and Wild,J. (1984) Rapid chemical degradation sequencing. *Biotechniques*, **2**, 2.
39. West,A.G., Causier,B.E., Davies,B. and Sharrocks,A.D. (1998) DNA binding and dimerisation determinants of *Antirrhinum majus* MADS-box transcription factors. *Nucleic Acids Res.*, **26**, 5277–5287.
40. Schwarz-Sommer,Z., Hue,I., Huijser,P., Flor,P.J., Hansen,R., Tetens,F., Lonnig,W.E., Saedler,H. and Sommer,H. (1992) Characterization of the *Antirrhinum* floral homeotic MADS-box gene *DEFICIENS* – evidence for DNA-binding and autoregulation of its persistent expression throughout flower development. *EMBO J.*, **11**, 251–263.
41. Tröbner,W., Ramirez,L., Motte,P., Hue,I., Huijser,P., Lönnig,W.E., Saedler,H., Sommer,H. and Schwarz-Sommer,Z. (1992) *GLOBOSA* – a homeotic gene which interacts with *DEFICIENS* in the control of *Antirrhinum* floral organogenesis. *EMBO J.*, **11**, 4693–4704.
42. Winter,K.U., Weiser,C., Kaufmann,K., Bohne,A., Kirchner,C., Kanno,A., Saedler,H. and Theißen,G. (2002) Evolution of class B floral homeotic proteins: obligate heterodimerization originated from homodimerization. *Mol. Biol. Evol.*, **19**, 587–596.
43. Huang,H., Mizukami,Y., Hu,Y. and Ma,H. (1993) Isolation and characterization of the binding sequences for the product of the *Arabidopsis* floral homeotic gene *AGAMOUS*. *Nucleic Acids Res.*, **21**, 4769–4776.
44. Huang,H., Tudor,M., Su,T., Zhang,Y., Hu,Y. and Ma,H. (1996) DNA binding properties of two *Arabidopsis* MADS domain proteins: binding consensus and dimer formation. *Plant Cell*, **8**, 81–94.
45. Huang,H., Tudor,M., Weiss,C.A., Hu,Y. and Ma,H. (1995) The *Arabidopsis* MADS-box gene *AGL3* Is widely expressed and encodes a sequence-specific DNA-binding protein. *Plant Mol. Biol.*, **28**, 549–567.
46. Shiraishi,H., Okada,K. and Shimura,Y. (1993) Nucleotide sequences recognized by the AGAMOUS MADS domain of *Arabidopsis thaliana in vitro*. *Plant J.*, **4**, 385–398.
47. Messenguy,F. and Dubois,E. (2003) Role of MADS box proteins and their cofactors in combinatorial control of gene expression and cell development. *Gene*, **316**, 1–21.
48. Hochschild,A. and Ptashne,M. (1986) Cooperative binding of lambda repressors to sites separated by integral turns of the DNA helix. *Cell*, **44**, 681–687.
49. Tsai,S.Y., Tsai,M.J. and O'Malley,B.W. (1989) Cooperative binding of steroid hormone receptors contributes to transcriptional synergism at target enhancer elements. *Cell*, **57**, 443–448.
50. Kleinschmidt,C., Tovar,K. and Hillen,W. (1991) Computer simulations and experimental studies of gel mobility patterns for weak and strong non-cooperative protein binding to two targets on the same DNA: application to binding of tet repressor variants to multiple and single tet operator sites. *Nucleic Acids Res.*, **19**, 1021–1028.
51. Carey,J. (1988) Gel retardation at low pH resolves trp repressor-DNA complexes for quantitative study. *Proc. Natl Acad. Sci. USA*, **85**, 975–979.
52. Krämer,H., Niemöller,M., Amouyal,M., Revet,B., von Wilcken-Bergmann,B. and Müller-Hill,B. (1987) lac repressor forms loops with linear DNA carrying two suitably spaced lac operators. *EMBO J.*, **6**, 1481–1491.
53. Schleif,R. (1992) DNA looping. *Annu. Rev. Biochem.*, **61**, 199–223.
54. Purugganan,M.D., Rounsley,S.D., Schmidt,R.J. and Yanofsky,M.F. (1995) Molecular evolution of flower development - diversification of the plant MADS-box regulatory gene family. *Genetics*, **140**, 345–356.
55. Yang,Y.Z., Fanning,L. and Jack,T. (2003) The K domain mediates heterodimerization of the *Arabidopsis* floral organ identity proteins APETALA3 and PISTILLATA. *Plant J.*, **33**, 47–59.
56. Theißen,G., Kim,J.T. and Saedler,H. (1996) Classification and phylogeny of the MADS-box multigene family suggest defined roles of MADS-box gene subfamilies in the morphological evolution of eukaryotes. *J. Mol. Evol.*, **43**, 484–516.
57. Ma,H., Yanofsky,M.F. and Meyerowitz,E.M. (1991) *AGL1-AGL6*, an *Arabidopsis* gene family with similarity to floral homeotic and transcription factor genes. *Gene Dev.*, **5**, 484–495.
58. Kaufmann,K., Melzer,R. and Theissen,G. (2005) MIKC-type MADS-domain proteins: structural modularity, protein interactions and network evolution in land plants. *Gene*, **347**, 183–198.
59. Agrawal,N.J., Radhakrishnan,R. and Purohit,P.K. (2008) Geometry of mediating protein affects the probability of loop formation in DNA. *Biophys. J.*, **94**, 3150–3158.
60. Zhu,X.S., Linhoff,M.W., Li,G., Chin,K.C., Maity,S.N. and Ting,J.P. (2000) Transcriptional scaffold: CIITA interacts with NF-Y, RFX, and CREB to cause stereospecific regulation of the class II major histocompatibility complex promoter. *Mol. Cell Biol.*, **20**, 6051–6061.
61. Makeev,V.J., Lifanov,A.P., Nazina,A.G. and Papatsenko,D.A. (2003) Distance preferences in the arrangement of binding motifs and hierarchical levels in organization of transcription regulatory information. *Nucleic Acids Res.*, **31**, 6016–6026.
62. Hittinger,C.T. and Carroll,S.B. (2007) Gene duplication and the adaptive evolution of a classic genetic switch. *Nature*, **449**, 677–681.
63. Williams,T.M., Selegue,J.E., Werner,T., Gompel,N., Kopp,A. and Carroll,S.B. (2008) The regulation and evolution of a genetic switch controlling sexually dimorphic traits in Drosophila. *Cell*, **134**, 610–623.
64. Hill,T.A., Day,C.D., Zondlo,S.C., Thackeray,A.G. and Irish,V.F. (1998) Discrete spatial and temporal *cis*-acting elements regulate transcription of the *Arabidopsis* floral homeotic gene *APETALA3*. *Development*, **125**, 1711–1721.
65. Tilly,J.J., Allen,D.W. and Jack,T. (1998) The CArG boxes in the promoter of the *Arabidopsis* floral organ identity gene *APETALA3* mediate diverse regulatory effects. *Development*, **125**, 1647–1657.
66. Lee,J.Y., Baum,S.F., Alvarez,J., Patel,A., Chitwood,D.H. and Bowman,J.L. (2005) Activation of *CRABS CLAW* in the nectaries and carpels of *Arabidopsis*. *Plant Cell*, **17**, 25–36.
67. Gomez-Mena,C., de Folter,S., Costa,M.M.R., Angenent,G.C. and Sablowski,R. (2005) Transcriptional program controlled by the

floral homeotic gene *AGAMOUS* during early organogenesis. *Development*, **132**, 429–438.
68. Simonis,M., Kooren,J. and de Laat,W. (2007) An evaluation of 3C-based methods to capture DNA interactions. *Nat. Methods*, **4**, 895–901.
69. Dekker,J., Rippe,K., Dekker,M. and Kleckner,N. (2002) Capturing chromosome conformation. *Science*, **295**, 1306–1311.
70. Gustafson-Brown,C., Savidge,B. and Yanofsky,M.F. (1994) Regulation of the *Arabidopsis* floral homeotic gene *APETALA1*. *Cell*, **76**, 131–143.
71. Kempin,S.A., Savidge,B. and Yanofsky,M.F. (1995) Molecular basis of the cauliflower phenotype in *Arabidopsis*. *Science*, **267**, 522–525.
72. Wagner,D., Sablowski,R.W.M. and Meyerowitz,E.M. (1999) Transcriptional activation of *APETALA1* by LEAFY. *Science*, **285**, 582–584.
73. Mandel,M.A. and Yanofsky,M.F. (1998) The *Arabidopsis AGL9* MADS box gene is expressed in young flower primordia. *Sex Plant Reprod.*, **11**, 22–28.
74. Lebrecht,D., Foehr,M., Smith,E., Lopes,F.J., Vanario-Alonso,C.E., Reinitz,J., Burz,D.S. and Hanes,S.D. (2005) Bicoid cooperative DNA binding is critical for embryonic patterning in Drosophila. *Proc. Natl Acad. Sci. USA*, **102**, 13176–13181.
75. Ptashne,M. (2004) *A Genetic Switch – Phage Lambda Revisited*, 3rd edn. Cold Spring Harbor Laboratory Press, Cold Spring Harbor, New York.
76. Yang,Y.Z. and Jack,T. (2004) Defining subdomains of the K domain important for protein-protein interactions of plant MADS proteins. *Plant Mol. Biol.*, **55**, 45–59.
77. Riechmann,J.L., Krizek,B.A. and Meyerowitz,E.M. (1996) Dimerization specificity of *Arabidopsis* MADS domain homeotic proteins APETALA1, APETALA3, PISTILLATA, and AGAMOUS. *Proc. Natl Acad. Sci. USA*, **93**, 4793–4798.
78. Zachgo,S., de Andrade Silva,E., Motte,P., Tröbner,W., Saedler,H. and Schwarz-Sommer,Z. (1995) Functional analysis of the *Antirrhinum* floral homeotic *DEFICIENS* gene in vivo and in vitro by using a temperature-sensitive mutant. *Development*, **121**, 2861–2875.